

Discrete Element Modeling (DEM) of the Vertically Vibrated Particle Bed

Muddasar Habib , Unsia Habib , Jamil Ahmed , Nusruth B. Mohabuth , Paul Langston , Nicolas J. Miles & Philip Hall

To cite this article: Muddasar Habib , Unsia Habib , Jamil Ahmed , Nusruth B. Mohabuth , Paul Langston , Nicolas J. Miles & Philip Hall (2014) Discrete Element Modeling (DEM) of the Vertically Vibrated Particle Bed, Particulate Science and Technology, 32:3, 257-273, DOI: [10.1080/02726351.2013.855685](https://doi.org/10.1080/02726351.2013.855685)

To link to this article: <https://doi.org/10.1080/02726351.2013.855685>



Accepted author version posted online: 23 Oct 2013.
Published online: 21 Mar 2014.



Submit your article to this journal 



Article views: 169



View Crossmark data 



Citing articles: 1 View citing articles 

Discrete Element Modeling (DEM) of the Vertically Vibrated Particle Bed

MUDDASAR HABIB,¹ UNSIA HABIB,¹ JAMIL AHMED,¹ NUSRUTH B. MOHABUTH,³ PAUL LANGSTON,² NICOLAS J. MILES,⁴ and PHILIP HALL⁴

¹*Department of Chemical Engineering, University of Engineering and Technology, Peshawar, Pakistan*

²*Process and Environmental Research Division, Faculty of Engineering, University of Nottingham, UK*

³*FCC Environment, Northampton, UK*

⁴*Division of Engineering, University of Nottingham Ningbo China, Ningbo, P. R. China*

Discrete element modeling (DEM) is a computational tool used for detailed exploration of dynamic particle bed behaviors. One such application is the analysis of finely sized particle mixtures under the influence of external forces such as vertical vibration, which is difficult, if barely at all accessible for detailed experimental analysis. Here, we examined the differential density dynamic particle bed behaviors, by the application of a modified two dimensional DEM-fluid model that incorporates the gravity and fluid effects, to replicate some of the important experimental based observations of segregation, heaping, tilting, high density particles on top and bottom, and partition cell separation. The simulation results compared favorably with the reported literature on the density segregation attributes such as high density particles on top at vertical vibration frequency of 6.3 and 7 Hz with corresponding dimensionless acceleration magnitude of 1.6 and 2, convection currents at vertical vibration frequency of 30, 40, and 30 with corresponding dimensionless acceleration magnitude of 3.5, 4, and 3, layer separation at vertical vibration frequency of 7 Hz with corresponding dimensionless acceleration magnitude 2 and partition cell separation at vertical vibration frequency of 45 Hz and corresponding dimensionless acceleration magnitude of 2.25 for simulated glass and bronze particle mixture properties.

Keywords: DEM, density segregation, high density particles on top and bottom, partition cell separation, tilting

1. Introduction

Most of the particle processing knowledge remains empirical and the poor understanding of how to model the particulate phenomena has resulted in the development of very few general design and analysis approaches. The particulate models based on kinetic theory include some constraining assumptions that limit the use of this approach to the whole range of the particulate phenomena (Campbell 1990). There is as of yet no equation of particle motion analogous to the Navier-Stokes equation for fluids (Yang 1999). The theories used for describing particulate flows contain many limiting assumptions, for example, particles are round, interparticle collisions are instantaneous and binary, the coefficient of restitution is constant, and the random motion of particles is independently distributed (Campbell 1990; Yang 1999). Furthermore, the laws on mechanics of interactions in particulate materials are generally derived from the appropriate statistical averaging (Chou 2000).

In the scenario of having many limiting assumptions for particulate theories, computer simulations and experiments provide a valuable tool to model the particulate phenomena (Kruggel-Emden et al. 2007). It appears that the renewed interest in the particulate material research is partly due to the development of powerful computer simulation tools that can now tackle thousands of particles with better reproducibility as the computer processing speeds and data storage capabilities have increased since 1980s (Wassgren 1997; Asmar et al. 2002; Kruggel-Emden et al. 2007). Computer simulations offer several important features for studying particulate materials such as, reduced processing times and costs, the most significant among all being that the state of the particulate system is known at all times (Fazekas 2007). Hence, the interior of a dynamic particle state, such as during vertical vibration, can be examined and measurements can be made that may be difficult to perform during the course of any real and/or physical experiments (Wassgren 1997; Fazekas 2007; Zhu et al. 2008). The highly discontinuous nature of particulate materials makes them a favorable choice for treatment by discrete methods (Yang 1999; Asmar et al. 2002; Fraige and Langston 2006; Rosato et al. 2002; Fazekas 2007; Zhu et al. 2008). The term “discrete” refers to the fact that the DEM computer simulation models particulate materials as a system of individual particles (Wassgren 1997). Many computational methods such as

Monte Carlo techniques (Fan and Tang 2007), Cellular Automata, and the hard and soft particle models (Wassgren 1997) including the different variants of distinct/discrete element modeling (DEM) introduced by Cundall and Strack in 1979 (Tijskens et al. 2003; Fazekas 2007), uses the discrete element/particle based simulation approach (Herrmann and Ludding 1998).

Computer simulations based on DEM incorporate concepts from various domains of discrete geometry, theoretical physics and numerical computing (Wassgren 1997; Fazekas 2007). The main advantage offered by a DEM simulation is that the highly complex systems such as particle conveyers, particle mixing and segregation can be modeled with basic data without the need of any oversimplifying assumptions (Asmar et al. 2002; Fraige and Langston 2006; Zhu et al. 2008). In DEM, the trajectory of each participating element/particles is calculated from its interactions with other the elements/particles, interstitial fluid and with external factors such as gravitational, electrical, and magnetic fields (Wassgren 1997; Yang 1999; Fazekas 2007; Zhu et al. 2008).

Biswas et al. (2003) have used the three dimensional soft-sphere based molecular dynamic technique to model the finely and parallel sized binary particle mixtures that were vertically vibrated in the presence of air which replicated most of their experimentally observed particle segregation phenomena. Zeilstra et al. (2006) have used a numerical simulation based hybrid particle dynamic and computational fluid dynamic models to simulate the air induced segregation of the equal sized bronze and glass particles. Their (Zeilstra et al. 2006) computer simulations reproduced many of the commonly observed particle segregation behaviors such as bronze on top (in a vertical vibration time of 2.6 sec) and bronze sandwich configurations (in a vertical vibration time of 21 sec) with the magnitudes of vertical vibration frequency and dimensionless acceleration in the range of 55–130 Hz and 10–11, respectively. Among others, the particle segregation behaviors simulated by Zeilstra et al. (2006) with parallel particle mixtures were experimentally observed by Burtally et al. (2002, 2003). Other examples of DEM simulation techniques investigating the side wall induced particle convection cells in the vertically vibrating particulate systems can be seen in the work of Gallas et al. (1992), Taguchi, (1992), and Lee (1994).

Most of the DEM simulations are carried in two instead of three dimensions mainly because of the need of less number of computations and memory storage requirements (Wassgren 1997; Gallas et al. 1992; Taguchi 1992; Asmar et al. 2002). The coordinate system used in this DEM simulation work is shown in Figure 1.

Computer simulations carried in two dimensions have produced results that are comparable with the real three-dimensional system experiments for example, the shaking of particles in a container (Wassgren 1997; Gallas et al. 1992; Taguchi 1992; Zhu et al. 2008).

The main purpose of a DEM simulation is to get some insight into the behavior of a large assembly of discrete particles hence the use of sufficient number of particles in the computer simulation is important (Wassgren 1997). However,

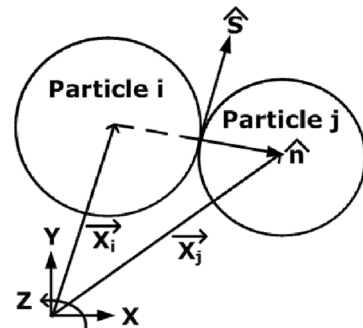


Fig. 1. Coordinate system used in the DEM simulation.

what constitutes a sufficient number of particles in a computer simulation is still open to debates. The use of too few particles can result in non-representation of a real particulate system however, on occasions the use of few particles is aimed to minimize the computational costs (Wassgren 1997).

The DEM simulation starts with an initial configuration of a physical particulate system. The usual DEM simulated systems have open boundaries however, periodic boundary conditions to imitate the large particulate systems can also be used (Fazekas 2007). Most of the particulate systems simulated by DEM consist of two-dimensional circular disks in the planar and/or cylindrical walls however, more complex objects such as polygonal, polyhedral, cubical (Fraige et al. 2008) and ring-shaped elements can also be modeled by DEM (Fazekas 2007; Wassgren 1997). In DEM, the use of two dimensional circular disks can result in an easy detection of the particle-particle and particle-wall collisions, particle overlaps and the location of contact points during the inter-particle and side wall collisions (Wassgren 1997; Fazekas 2007). Furthermore, circular particles are used in DEM as the kinetic theories for dynamic particles have assumed spherical and/or circular-shaped particles (Wassgren 1997). Nevertheless, the resulting conclusions derived from the DEM simulations of cylindrical and/or spherical-shaped particles are often considered to hold for the other kind of particle shapes (Lehon et al. 2003).

In a soft particle model based DEM simulation approach, the forces are generally classified as either body or contact forces (Wassgren 1997). Body forces such as gravitation and/or electromagnetic fields typically act on all dynamic particles (Wassgren 1997). However, the contact forces such as cohesive, elastic, friction, and damping forces are event driven and act only when the particles are in a contact (Wassgren 1997; Asmar et al. 2002; Fraige and Langston 2006). In a two-dimensional simulation system, the contact forces are usually modeled in the normal and tangential directions (Asmar et al. 2002). Interstitial fluid forces are the third type of force that can also be included in the soft particle based DEM simulations (Wassgren 1997). The force calculations in DEM are based on the principle that during a small time step, the particle forces and accelerations can be assumed constant, while the particle velocities are allowed to vary linearly hence, the selection of a simulation time step is crucial to maintain the stability and accuracy of the

simulation algorithm (Asmar et al. 2002; Fraige and Langston 2006).

In DEM, the particles are moved to new locations by solving the Newton's equation of particle motion (Fazekas 2007). The force calculation and integration procedure is repeated several times and the data can either be processed during the course of a simulation run to create the computer animations or can be stored for later evaluation (Fazekas 2007).

Based on the stated importance of understanding the dynamic particle behaviors, the work presented here investigates the application of a DEM-fluid simulation program, originally developed by Langston, Fraige, and Asmar (Asmar et al. 2002; Fraige and Langston 2006), that was modified to model the vertically vibrating particles in a confined container in the presence of air. This work was aimed to replicate some of the important experiment based (Burtally et al. 2002; Burtally et al. 2003; Mohabuth and Miles 2005; Mohabuth 2007; Mohabuth et al. 2007; Habib 2011) dynamic particle attributes such as particle bed heaping, tilting, convection currents, and segregation under the influence of vertical vibration.

2. The Applied DEM Model

This work has modeled the circular-shaped particles with linear interactions as these particle shapes were considered to best represent the spherical shape features of the particles used in the real and/or physical experiments reported by Burtally et al. (2002, 2003), Mohabuth and Miles (2005), Mohabuth et al. (2007), and Mohabuth (2007). Note that instead of simulating circular disks, the DEM simulation models particles as spheres constrained to move in two dimensions. The difference between using the disks or spheres appears only in the moment of inertia of the particles (Wassgren 1997). The moment of inertia for a circular disk is $1/2(mr^2)$ and that for a sphere is $2/5(mr^2)$, where m , is the

mass of the particle and r is the particle radius. The equations representing the moment of inertia of a particle shows that the spheres rotate more easily in comparison to disks. The mass, m of a spherical particle can be represented by Equation (1),

$$m = \rho \frac{4}{3} \pi r^3 \quad (1)$$

where ρ represents the particle density, r is a particle radius and $\pi = 3.14$ is a mathematical constant whose value is the ratio of a circle's area to the square of its radius. If the DEM simulations are modeled to consider only the inter-particle and body forces, the mass and density of a spherical and/or disk-shaped particle does not affect the simulation results. However, if other forces such as electrostatic and/or interstitial fluid forces are considered then the mass of a spherical particle (Equation (1)) could potentially become important as it would significantly affect the momentum of the individual particles (Wassgren 1997). Variants of DEM simulations differ mainly in the way in which the inter-particle interactions (hard and soft-body) are calculated (Fazekas 2007). In this DEM work, a soft body inter particle interaction approach (proven effective in modeling dense flows) has been used.

2.1 Construction of a Discrete Geometry

Handling the high level of discreteness in the particulate system makes DEM simulation an algorithmically complex problem (Fazekas 2007). The simplest way to find the particles that are close to each other is to divide the simulation space into cells of a given size and assign each particle to the cell in which its centre point is located (Fazekas 2007; Asmar et al. 2002). Different geometric constructs that are normally used to speed up the detection of the interacting particles are shown in Figure 2.

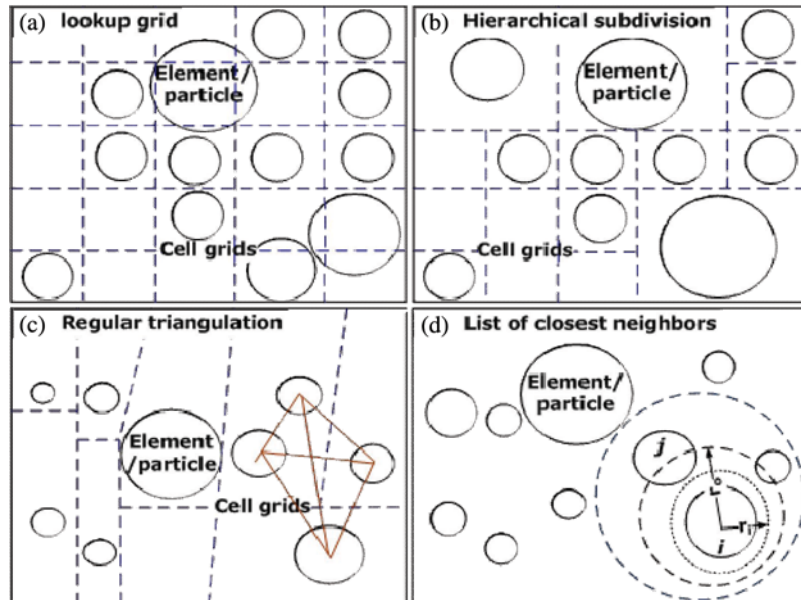


Fig. 2. Geometric constructs/grids which are used to speed up the detection of the interacting particle pairs (Fazekas 2007).

It is a norm in DEM to assume that in a single time step the disturbances cannot propagate further than the immediate neighbor of a single particle (Asmar et al. 2002). This assumption has proved less defective in comparison to other usual assumptions of using the spherical-shaped particles and not modeling the dynamic particle breakages (Asmar et al. 2002).

The DEM work reported here has used the list of close neighbors (Figure 2) geometric construct and/or grid structure to speed up the detection of the interacting particle pairs.

2.2 Particle Contact Models

The widely used soft sphere contact model in DEM is the so-called linear spring-dashpot model (Wassgren 1997; Fazekas 2007). The selection of a soft sphere model, as used in this work, was based on the fact that most of the real particles used in the vertically vibrating particulate systems experience multiple and long duration particle-particle and particle-wall contacts, at-least for part of an oscillation cycle. This point rules out the use of a hard sphere contact model in this work. The soft sphere based linear spring dashpot contact model is based on the idea that when a contact relative to the surface orientation is established between the two particles, a normal and tangential spring is created at the initial contact point (Fazekas 2007). The motion of particles is then assumed to govern by the elongation of these imaginary springs and the springs act until the particles separate from each other (Fazekas 2007). The schematic of a soft sphere based linear dashpot contact force model is shown in Figure 3.

In Figure 3, the springs provide a restoring force that tries to push the particles apart, and the dashpot provides the dissipation energy that makes the collisions inelastic (Wassgren 1997). In addition, a friction slider with an associated friction coefficient μ is added in series with the tangential-direction spring and dash-port so that there is no tangential slippage between the particles as long as the tangential force is smaller than μ times the normal force (Figure 3). If this value is exceeded, the particles will slip with a force equal to μ times the normal force (Wassgren 1997).

2.3 Particle Contact Forces

The total force on a particle consists of a constant gravitational acceleration and the forces exerted over the points

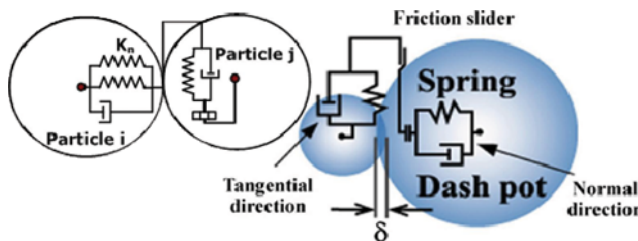


Fig. 3. Schematic diagram of contact forces that are modeled by using a soft sphere based linear spring-dashpot model (Wassgren 1997; Asmar et al. 2002; Fazekas 2007).

of contact with its immediate neighbors and the boundary walls of the simulation (Fazekas 2007). In this work the normal and tangential components of force (F_n and F_t , respectively) which the particles in contact exert on each other, is modeled by Equations (2) and (3),

$$F_n = -K_n u_n - \gamma_n v_n \quad (2)$$

$$F_t = -K_t u_t - \gamma_t v_t \quad (3)$$

where $K_{n,t}$ and $\gamma_{n,t}$ are the normal and tangential stiffness and damping coefficients, u_n and u_t are the normal and tangential displacements relative to the initial contact point (elongation point of the spring), and v_n and v_t are the relative velocities at contact point of the arbitrarily translating and rotating particles (Fazekas 2007). The normal displacement, measured along the direction perpendicular to the surface of the particles in contact, depends on the relative position, size, and shape of the particles (Fazekas 2007), for example, in case of two spheres this can be represented by Equation (4),

$$u_n = R_1 + R_2 - ||r_1 - r_2|| \quad (4)$$

where $R_{1,2}$ are the radii of spheres and $r_{1,2}$ are the centre points. Equation (4) is non-negative as long as the spheres overlap (Fazekas 2007). When u_n becomes negative, the bodies do not touch each other and no contact force should act between them (Fazekas 2007).

The tangential displacement u_t is calculated by integrating the tangential velocity v_t in the contact plane during the lifetime of the contact by using Equation (5).

$$u_t(t) = \int v_t(t) dt \quad (5)$$

In two dimensions the tangential displacement, u_t and the tangential velocity, v_t (Equation (5)) is represented as scalars (Fazekas 2007). Care must be taken to avoid ghost forces, instabilities, and spurious dissipation (Fazekas 2007). According to the Coulomb's rule, any friction force which act in the tangential direction, F_t must obey the constraint given in Equation (6),

$$||F_t|| \leq \mu ||F_n|| \quad (6)$$

where μ is the coefficient of friction between the two sliding surfaces (Fazekas 2007). In order to satisfy the Coulomb's rule (Equation (6)), F_t is shortened when its magnitude becomes too large, while its direction is kept the same (Fazekas 2007). For modeling sliding contacts, the elongation of the tangential spring F_t is relaxed to $\mu ||F_n||/k_t$ accordingly (Fazekas 2007).

In this work, a linear spring dashpot model as shown in Figure 3 is used to calculate the particle-particle and particle-wall contact forces. The normal contact force F_N of the model is given by Equation (7)

$$F_N = F_{NE} + F_c + F_{ND} \quad (7)$$

where F_{NE} is the normal elastic force, F_c is the cohesion force and F_{ND} is the normal damping force. The tangential contact force F_T is limited by the coulomb's frictional limit to the point where the surface contact shears and the particles begin to slide over each other (gross sliding). The tangential

contact force F_T is given by Equations (8) and (9).

$$F_T = F_{Fbgs} + F_{TD}, \text{ below the Coulomb's frictional limit} \quad (8)$$

$$F_T = F_{Fags}, \text{ above the Coulomb's frictional limit} \quad (9)$$

where F_{Fbgs} is the elastic component of friction force prior to gross sliding, F_{TD} is the tangential damping force, and F_{Fags} is the friction force at and after gross sliding (Asmar et al. 2002; Fraige and Langston 2006).

2.3.1 Normal Elastic Force

The normal elastic force F_{NE} , which represents the repulsive force between any two particles, is calculated by using the Hook's linear spring relationship as given by Equation (10),

$$F_{NE} = K_N \delta_N \quad (10)$$

where K_N is the spring stiffness in the normal direction and δ_N is the displacement between particles i and j as shown in Figure 3. The maximum particle overlap is desired around 0.1 to 1.0% which requires spring stiffness K_N to be in the order of 10^6 – 10^7 N/m (Asmar et al. 2002).

2.3.2 Normal Damping Force

The normal damping force F_{ND} is modeled as a dashpot that dissipates a portion of the relative kinetic energy (Asmar et al. 2002; Fraige and Langston 2006) as estimated by Equation (11),

$$F_{ND} = C_N v_N \quad (11)$$

where v_N is the normal component of the relative velocity and C_N is the normal damping coefficient, which can be chosen to give a required coefficient of restitution ε which is defined as the ratio of the normal component of relative velocities before and after collision. Although each particle can have a different coefficient of restitution however, in the general DEM modeling practice a sole value for all particles is used (Asmar et al. 2002).

The normal damping coefficient C_N is estimated by Equation (12),

$$C_N = 2\gamma \sqrt{m_{ij} K_N} \quad (12)$$

where γ is the coefficient of critical damping and is calculated by Equation (13).

$$\gamma = \frac{\ln(\varepsilon)}{\sqrt{\pi^2 + \ln^2(\varepsilon)}} \quad (13)$$

where m_{ij} in Equation (12) is estimated by Equation (14),

$$m_{ij} = \frac{m_i m_j}{m_i + m_j} \quad (14)$$

where m_{ij} is the mass of the particles i and j .

2.3.3 Friction Force

The variation in friction force prior to gross sliding F_{Fbgs} is calculated by using the Hook's linear spring relationship as given by Equation (15),

$$F_{Fbgs} = K_T \delta_T \quad (15)$$

where K_T is the tangential stiffness coefficient and δ_T is the total tangential displacement between the two particle surfaces since

their initial contact (Asmar et al. 2002). As mentioned, the total tangential force is limited by the Coulomb's frictional limit. If δ_T exceeds δ_{Tmax} then sliding occurs and δ_T does not increase. In this DEM simulation, the friction force after gross sliding F_{Fags} is calculated by using Equation (16),

$$F_{Fags} = \mu F_{NE} \quad (16)$$

where μ is the coefficient of friction and F_{NE} is the normal elastic force. δ_{Tmax} can be estimated by Equation (17) as,

$$\delta_{Tmax} = \delta_R \delta_N \quad (17)$$

where δ_R is a constant and δ_N is the total normal displacement. It has been shown that δ_R , which couples the tangential displacement to normal displacement, can be calculated as a function of Poisson's ratio ν and the coefficient of friction μ of the particles (Asmar et al. 2002).

2.3.4 Tangential Damping Force

The tangential damping force F_{TD} (Equation (18)) is modeled as a dashpot that dissipates energy as a result of the tangential particle motion. The tangential damping force F_{TD} can be represented by Equation (18),

$$F_{TD} = C_T v_T \quad (18)$$

where v_T is the tangential component of relative velocity between the particles and C_T is the tangential damping coefficient. The tangential damping coefficient C_T , calculated by Equation (19), is chosen to give a specified coefficient of restitution ε which is defined as the ratio of post- to pre-collision tangential component of the relative velocity.

$$C_T = 2\gamma \sqrt{m_{ij} K_T} \quad (19)$$

In Equation (19), γ and m_{ij} are the same as represented in Equations (13) and (14). When gross sliding occurs then the value of $K_T = 0$ and in this situation the gross sliding F_{Fags} (Equation (16)) is the total force that dissipates energy from the tangential motion (Asmar et al. 2002).

2.3.5 Particle-Wall Contacts

Here, the interaction of a particle with the vessel wall is modeled in a similar manner as a particle-particle contact. Even when the particle is in contact with two walls, only one contact is generally simulated in DEM (Asmar et al. 2002). This assumption has proven to be less significant in comparison to the other assumptions that are routinely made in a DEM simulation (Asmar et al. 2002).

2.4 DEM Simulation Parameters

The DEM simulation parameters used in this work are classified into two major categories, based on the method in which they are chosen (Wassgren 1997; Asmar et al. 2002; Fazekas 2007). The first category is for parameters that are taken directly from the experiments such as gravitational acceleration g (9.8 m/sec²), and others calculated by the use of equations such as vertical vibration frequency f , as given by Equation (20),

$$f = \frac{\omega}{2\pi} \quad (20)$$

where ω is the angular frequency, Hz, π is a mathematical constant, and dimensionless vertical vibration acceleration Γ , as given by Equation (21),

$$\Gamma = \frac{a\omega^2}{g} \quad (21)$$

where a (m) is the oscillation amplitude, g (m/sec²) is the gravitational acceleration and ω is the angular frequency (Hz) given by Equation (22),

$$\omega = 2\pi f \quad (22)$$

where f is the frequency Hz, and π is a mathematical constant.

2.5 Modeling of External Forces in DEM

2.5.1 Gravitational Force

The gravitational force g is introduced as a constant linear force, of magnitude 9.8 m/sec², acting at the centre of each particle.

2.5.2 Vibration Force

Here the vibration force on the particle container is limited and/or confined to act in z direction only. The particles move as a result of a contact between the moving base wall and the surrounding particles. The particle's container movement is defined relative to the vessel base, which at any time is represented by Equations (23) and (24),

$$\text{for } t < t_{start}, Z_{base} = 0 \quad (23)$$

$$\text{for } t > t_{start}, Z_{base} = A \sin(f(t - t_{start})) \quad (24)$$

where A is the vibration amplitude, f is the vibration frequency, t is the vibration time, and t_{start} is the time when the vibration first starts.

2.5.3 Air Drag Calculation

The vertical vibration induced air drag on each particle is calculated by using Equation (25),

$$F_d = -\frac{\Delta P_p}{\Delta x} \left(\frac{V}{(1-\varepsilon)} \right) \quad (25)$$

where ΔP is estimated in the lean particle phase (for particle void fraction $\varepsilon > 0.8$) by Equation (26), first proposed by Wen and Yu in 1966 (Fraige and Langston 2006),

$$\beta = -\frac{\Delta P_{lp}}{\Delta x} = \frac{3}{4} \left(\frac{(1-\varepsilon)}{d} \right) C_D \rho f e^{-2.7} |u - \bar{v}| (u - \bar{v}) \quad (\text{wen and Yu, 1966}) \quad (26)$$

where ΔP_{lp} is the pressure drop in the lean particle phase, Δx is the length of the particle container, C_D is the coefficient of drag acting on a single particle, u is the interstitial gas velocity, \bar{v} is the average particle velocity and ε is the particle void fraction.

The pressure drop induced due to the presence of particles in the dense phase (for particle void fraction, $\varepsilon < 0.8$) is estimated by Equation (27), first proposed by Ergun in 1952 (Fraige and Langston 2006),

$$\beta = -\frac{\Delta P_{dp}}{\Delta x} = \frac{(1-\varepsilon)}{d\varepsilon^3} \left[150 \frac{(1-\varepsilon)}{d} \mu_f \varepsilon (u - \bar{v}) + 1.75 \rho f \varepsilon^2 |u - \bar{v}| (u - \bar{v}) \right] \quad (\text{Ergun, 1952}) \quad (27)$$

where ΔP_{dp} is the pressure drop in the dense particles phase and μ_f is the interstitial fluid viscosity. In this work, the particle void fraction ε for each grid cell is estimated by using the list of close neighbors (Figure 2) method.

The gas phase motion in this DEM is predicted by the Euler's equation (Equation (28)) of motion, which assumes the surrounding gas to be incompressible and in-viscid with no gravity and turbulence effects (Limtrakul et al. 2007).

$$\frac{\partial(\varepsilon \bar{u})}{\partial t} + \nabla \cdot (\varepsilon \bar{u} \bar{u}) = -\frac{\varepsilon \nabla p}{\rho} + \bar{f}_s \text{ where } \bar{f}_s = \frac{\beta}{\rho} (\bar{v}_p - \bar{u}) \quad (28)$$

where \bar{u} is the interstitial fluid velocity, \bar{f}_s is the force exerted by particles on the interstitial fluid, \bar{v}_p is the particle velocity vector and β is the same factor as given in Equations (26) and (27) for the lean and dense particle phases.

2.6 Integration of Particle Motion in DEM

The solution of Newton's equation of particle motion through a numerical scheme moves the particles to a new position from simulation step to the simulation step (Fazekas 2007). By considering the total and/or net force \mathbf{F} acting on a body of mass m the acceleration a of a particle is calculated by Equation (29).

$$a = F/m \quad (29)$$

With the Euler's method, the new position and/or displacement and velocity of the particle is calculated by using Equations (30) and (31)

$$r(t + \delta t) = r(t) + v(t)\delta t \quad (30)$$

$$v(t + \delta t) = v(t) + a(t)\delta t \quad (31)$$

where δ_t is a small time step. The new positions (Equation (30)) and velocities (Equation (31)) can be used to update the forces by repeating the procedure as many times as needed. The integration time scale δ_t can be either fixed or adapted to the dynamic time scale of the simulated system (Fazekas 2007). In two dimensions, the orientation of an arbitrarily shaped particle can be described by the rotation angle relative to the fixed direction and the Euler's method for computing the translational motion can be used to compute the particle's rotational motions (Fazekas 2007).

2.6.1 Translational Particle Motion

The translational particle motion is calculated by using the Newton's law of motion as given by Equation (32),

$$m_i \frac{dv}{dt} = F_G + \sum F_N + \sum F_T \quad (32)$$

where m is the mass of a single particle i , F_G is the gravitational force, $\sum F_N$ and $\sum F_T$ are the respective sums of all the normal and tangential forces (particle-particle and particle-wall) acting on a single particle and v is the linear

particle velocity. In this DEM work, the acceleration of a single particle is computed from the net force (Equation (29)) which is then integrated for particle velocity (Equation (30)) and displacement (Equation (31)).

2.6.2 Rotational Particle Motion

The rotational particle motion is calculated by using Equation (33),

$$I_i \frac{d\omega}{dt} = \sum M \quad (33)$$

where I is the moment of inertia of a particle, ω is the angular velocity, and M is the particle's momentum, calculated by Equation (34),

$$M = R \times F_T \quad (34)$$

where R is a radial vector which extends from the particle's centre to the point of contact and X is a vector cross product. In DEM, the trajectories of all the particles can be traced by integrating Equations (32) and (33). The simulation time step Δt is a constant value that is chosen to ensure the stability and accuracy of the numerical integration system (Asmar et al. 2002). The value of simulation time step Δt is often determined on the basis of maximum particle stiffness k , and the smallest particle mass, m as shown in Equation (35).

$$\Delta t \propto \sqrt{\frac{m}{k}} \quad (35)$$

In Equation (35), several values of proportional constant are suggested in literature such as 0.1, 2 and $2/10(\pi)$ (Asmar et al. 2002). However, it is sometimes necessary to conduct some simulation trial runs to evaluate the most appropriate time step value for use in a simulation system (Asmar et al. 2002). The selection of an inappropriate time step value can lead to the propagation of rounding error, artificial oscillations and unnecessarily long runtimes (Asmar et al. 2002).

3. DEM Input Parameters

The input variables needed to run this DEM simulation can be divided into three main groups and/or categories: the geometric data of the vertically vibrating particle container; the particle physical properties; and the required simulation output.

3.1 Group 1 Input Variables

Group 1 DEM input variables include the geometric vessel data such as the size and shape of the particle container and/or vessel. It includes the number of container sections, height, and width. In each DEM model, the position of the walls is defined with respect to the global coordinate system shown in Figure 1.

3.2 Group 2 Input Variables

These include the particle's physical properties such as the size, shape, and density.

3.3 Group 3 Output Variables

Depending on the objectives of the computer simulation study, a TRUE/FALSE Boolean value can be assigned to each possible output variable of the DEM simulation program.

4. DEM Implementation Code

The DEM simulation code used in this work was written in Visual Basic 6 and was divided into several logical subroutines. The DEM simulation flow chart is shown in Figure 4.

Figure 4 demonstrates that during the course of any computer simulations, the particle and simulation environment data is first read and then the particle initial conditions are determined. Next, the preliminary routines are called in from the DEM program and the main simulation loop begins. In the main simulation loop, the forces acting on each particle in the system are determined based on the selected particle contact model (soft particle method in this case). Once the force subroutine is finished, the particle equations of states are integrated and the appropriate measurements are made. Next, the particle states are recorded to an output file. The loop repeats until an ending condition, which is usually the maximum allowable simulation time, is reached.

All the DEM simulations reported in this work were run on a Viglen desktop personnel computer with an Intel Pentium (R)D 3.4 GHz processor with a 2GB RAM and a Microsoft XP professional version 2002 service pack 3 operating system.

4.1 DEM Validation Tests

Before the full scale running of the DEM simulation program, several validation tests were performed on the DEM simulation program to increase the confidence that the code has no mistakes:

1. large runs to inspect the overall running of the program.
2. manual calculations to check the small test runs.
3. inspection of the graphical output for step 1 and 3 to see if it looks sensible.

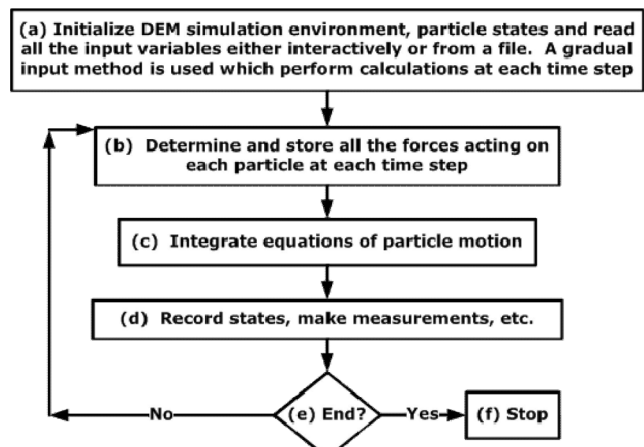


Fig. 4. DEM simulation flowchart.

4.2 DEM Simulation Setup

The rectangular-shaped container box representing the DEM simulation setup as used in this work is shown with dimensions in Figure 5.

The main simulation parameters, used in this DEM simulation setup (Figure 5), are summarized in Table 1.

5. Results and Discussion

5.1 DEM Simulation of the Vertically Vibrating Particle Mixtures

The simulation procedure in this DEM work is initiated by assigning random positions to the simulated working particles within the rectangular-shaped container as shown in Figure 5. The simulated particles are allowed to fall under gravity until a stable particle structure as shown in Figure 5 is obtained. In this DEM work, several experiments were performed to investigate the density segregation behavior of different spherical-shaped particles that were subjected to simulated vertical vibration.

5.2 Preliminary Density Segregation Simulations

The simulated working particle mixture used in the preliminary density segregation investigation is shown in Table 2.

The time averaged progression of vertical vibration induced particle segregation in the particle mixture shown in Table 2 at a vertical vibration frequency of 6.3 Hz and with a dimensionless acceleration magnitude of 1.6 is snapshot and shown in Figure 6.

The green particle in Figure 7 represents a high density tracer particle that is introduced into the simulation system to capture and highlight the distinct movements of the high density particles. The tracer particle is encircled in green for the ease of detection.

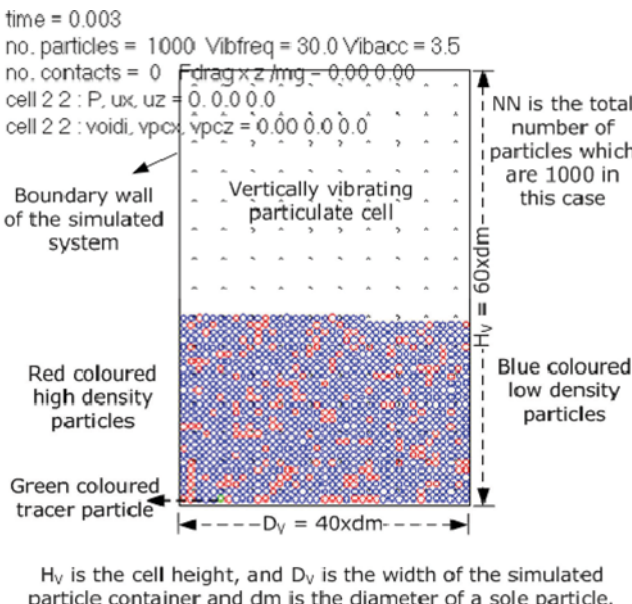


Fig. 5. DEM simulation setup.

Table 1. Parameters used in the DEM simulations

Parameter	Values
Number of particles, N	1000
Dimensionless acceleration, Γ	2.0, 3.0, 3.5, 4.0
Vertical vibration frequency, f (Hz)	6, 7, 9, 30, 35, 40, 45
Simulation boundaries	Walls
Particle density, ρ (kg/m ³)	(a) Glass (2.5), Bronze (8.9) and (b) Particles with the density of 1.0 and 2.5
Diameter of the particles, d_m (μm)	500 and 250
Maximum simulation time, t	30 sec
Average CPU time for 1 sec of simulation run	20 hrs
Interstitial gas	Air
Air viscosity, (kg/m · sec)	0.000018
Air density, (kg/m ³)	1.2
Gravity force, (m/sec ²)	9.8
Particle-particle stiffness coefficient, K_N (kg/sec ²)	250
Particle-wall stiffness coefficient, K_N , (kg/sec ²)	250
Particle-particle tangential stiffness coefficient, K_T (kg/sec ²)	250
Particle-wall tangential stiffness coefficient, K_T (kg/sec ²)	250
Particle-particle friction coefficient, μ	0.3
Particle wall friction coefficient, μ	0.3
Rolling friction, ($N = \text{kg}/\text{m} \cdot \text{sec}^2$)	0.0005
Particle-particle displacement ratio, δ_R	0.36
Particle wall displacement ratio, δ_R	0.36
Particle-particle normal damping coefficient, γ	0.3
Particle-wall normal damping coefficient, γ	0.3
Time step, Δt sec	0.001

Table 2. Size and density of the simulated working particle mixture used in the preliminary density segregation investigation

Bead diameter (μm)	Density $\rho(\text{kg}/\text{m}^3)$	Number ratio of particles
500	1000	0.3
500	2500	0.7
Total number of particles used in the DEM simulations		600 and 1000

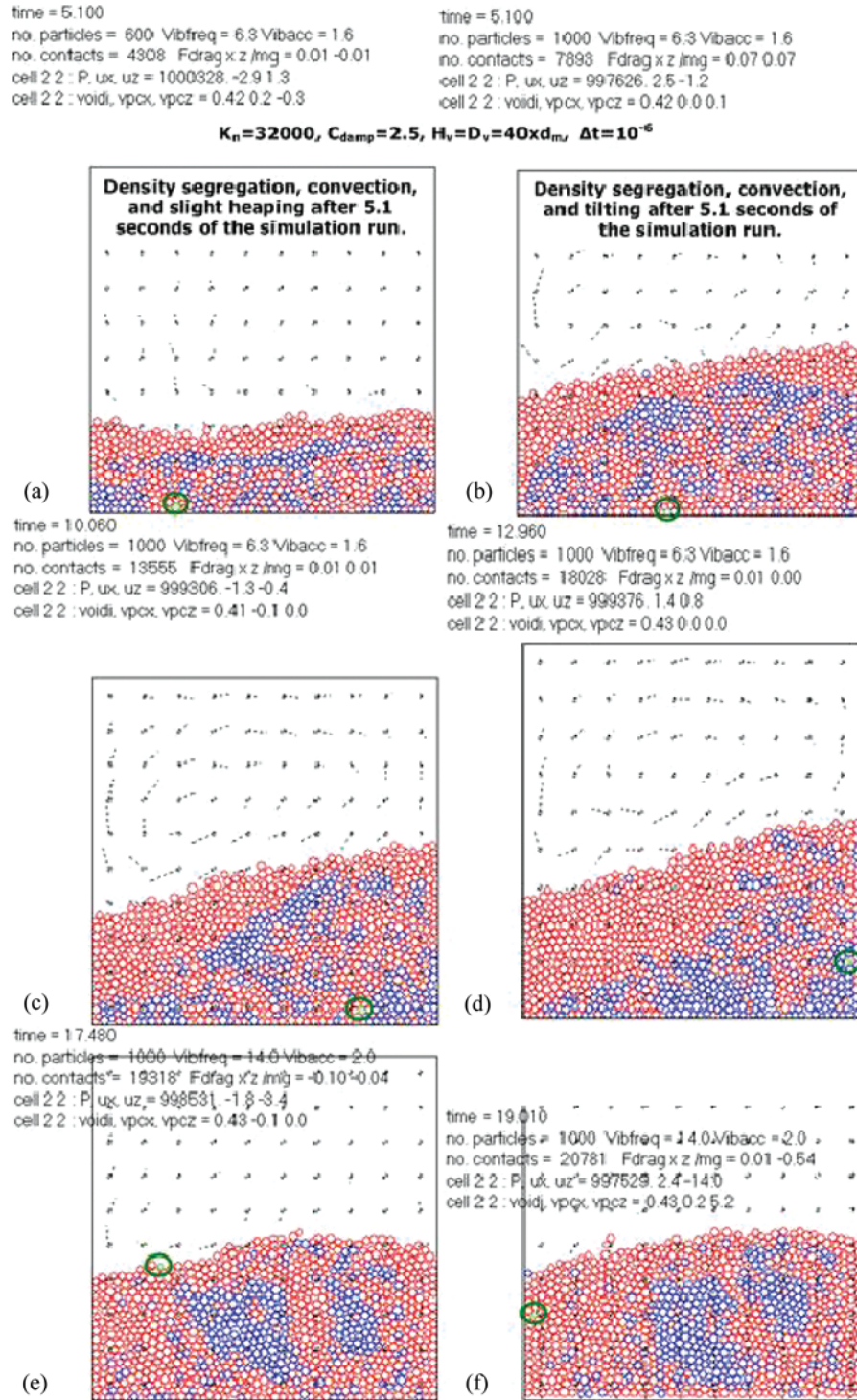


Fig. 6. DEM simulation of segregation progression in the 70:30% high and low density particle mixture (Table 2).

The DEM simulation (Figure 6) carried with particle mixture (Table 2) that contained 600 particles, showed (a) density segregation coupled with convective particle motions and slight heaping and/or tilting of the particle bed in nearly 5 sec of the simulation run. The DEM simulation results shown in Figure 6a were considered encouraging enough to simulate a further increase in the number of working particles. With everything else remained the same, the increase

in the number of particles to 1000 (Table 2) showed (b) similar particle segregation trends as seen in the simulation of 600 particles with the addition of a tilt formation that continued to remain stable even after (c) 10, (d) 13, (e) 17, and (f) 19 sec of the simulation run.

Of particular interest in the simulation run (Figure 6) carried with 1000 particles was the distinct movement of the green tracer particle which was initially housed in the

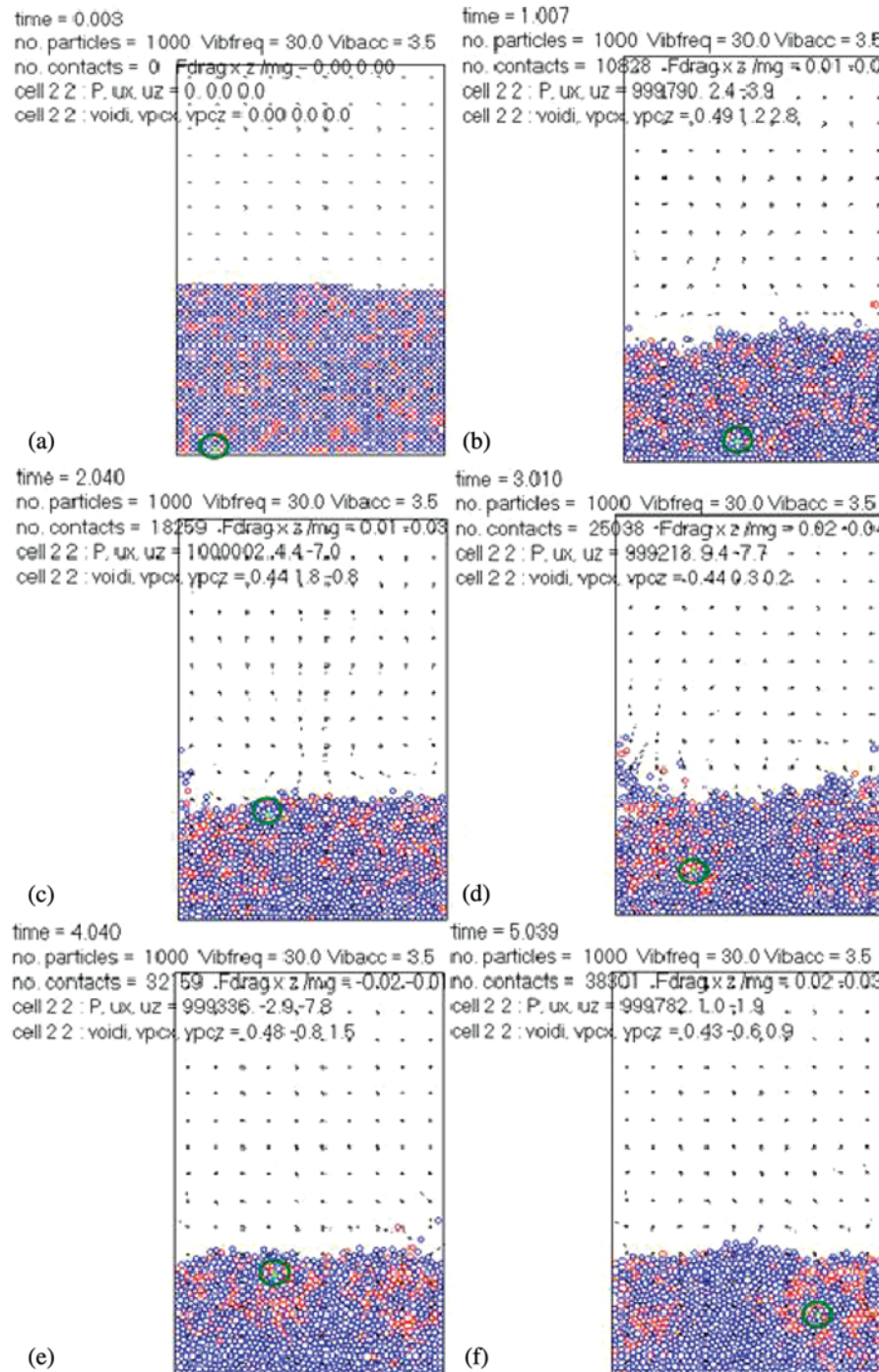


Fig. 7. DEM simulation of time averaged (from a to f, ~ 10 sec) segregation progression in an 80:20% number glass and bronze particle Mixture A (Table 3).

bottom layer of the simulated particles. As the vertical vibration started, the green tracer particle started to move towards the top of the tilted particle bed surface. However, during the course of this motion the tracer particle was observed to follow a trajectory that was very close to the boundary walls of the rectangular-shaped cell. Once on top, the tracer particle was observed to slide downhill from top of the tilted particle bed surface. Although the DEM simulations reported here replicated some of

the experimentally (Burtally et al. 2002; Burtally 2003; Mohabuth and Miles 2005; Mohabuth et al. 2007) observed density segregation attributes, however the use of a very low vertical vibration frequency and dimensionless acceleration magnitude as well as the use of a very low density differential particle mixture (Table 2) was considered far from agreement with most of the experimental conditions reported in literature such as the ones reported by Burtally et al. (2002; Burtally et al. 2003).

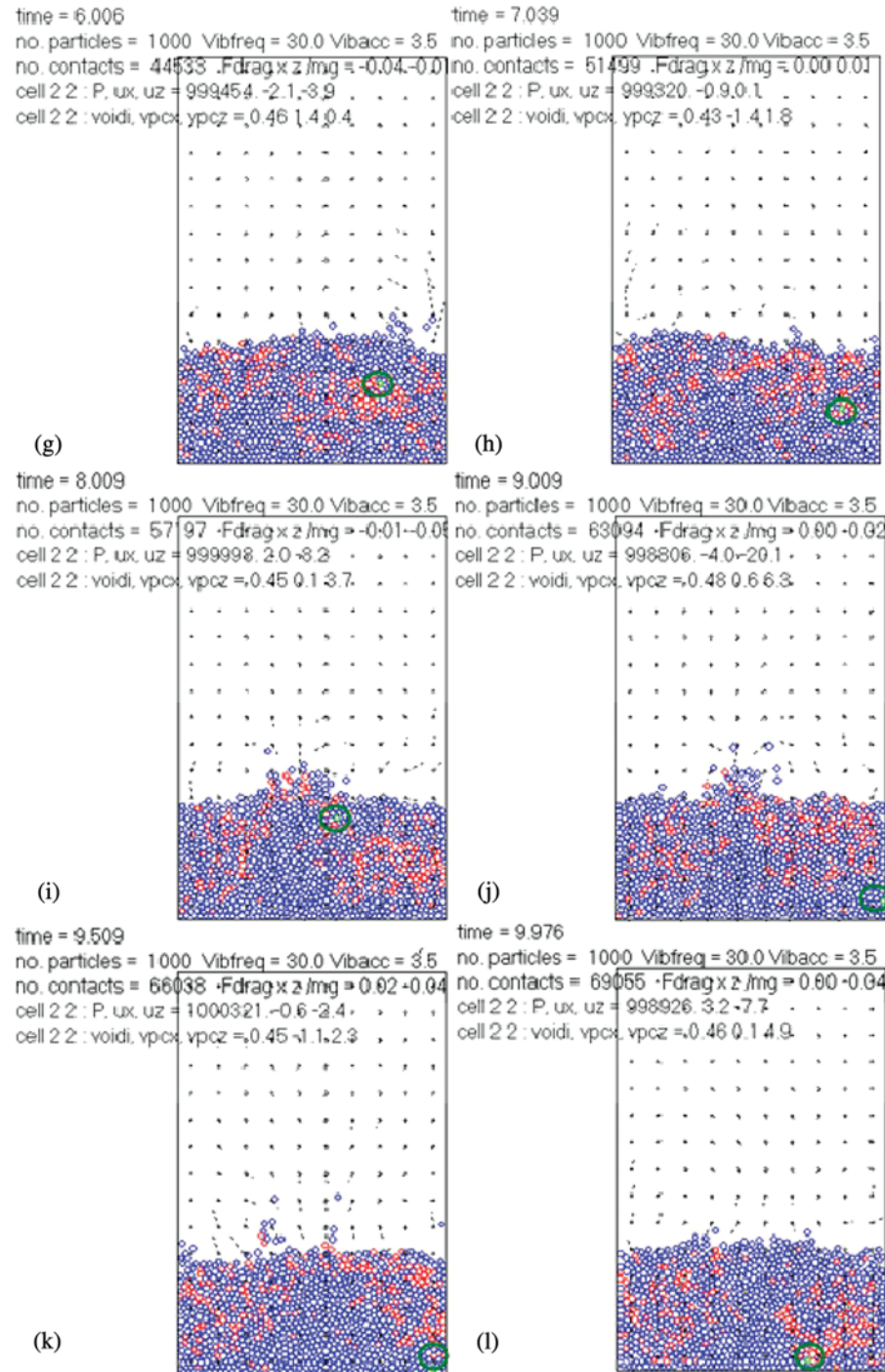


Fig. 7. Continued.

Table 3. Size and composition of the simulated working particle mixtures used in the DEM simulations

Mixture		A	B	C
Material	Bead diameter (μm)	Density $\rho(\text{kg}/\text{m}^3)$	Number ratio of particles	Number ratio of particles
Glass	500	2500	0.8	0.7
Bronze	500	8900	0.2	0.3
Total number of particles used in the DEM simulations		1000	1000	200

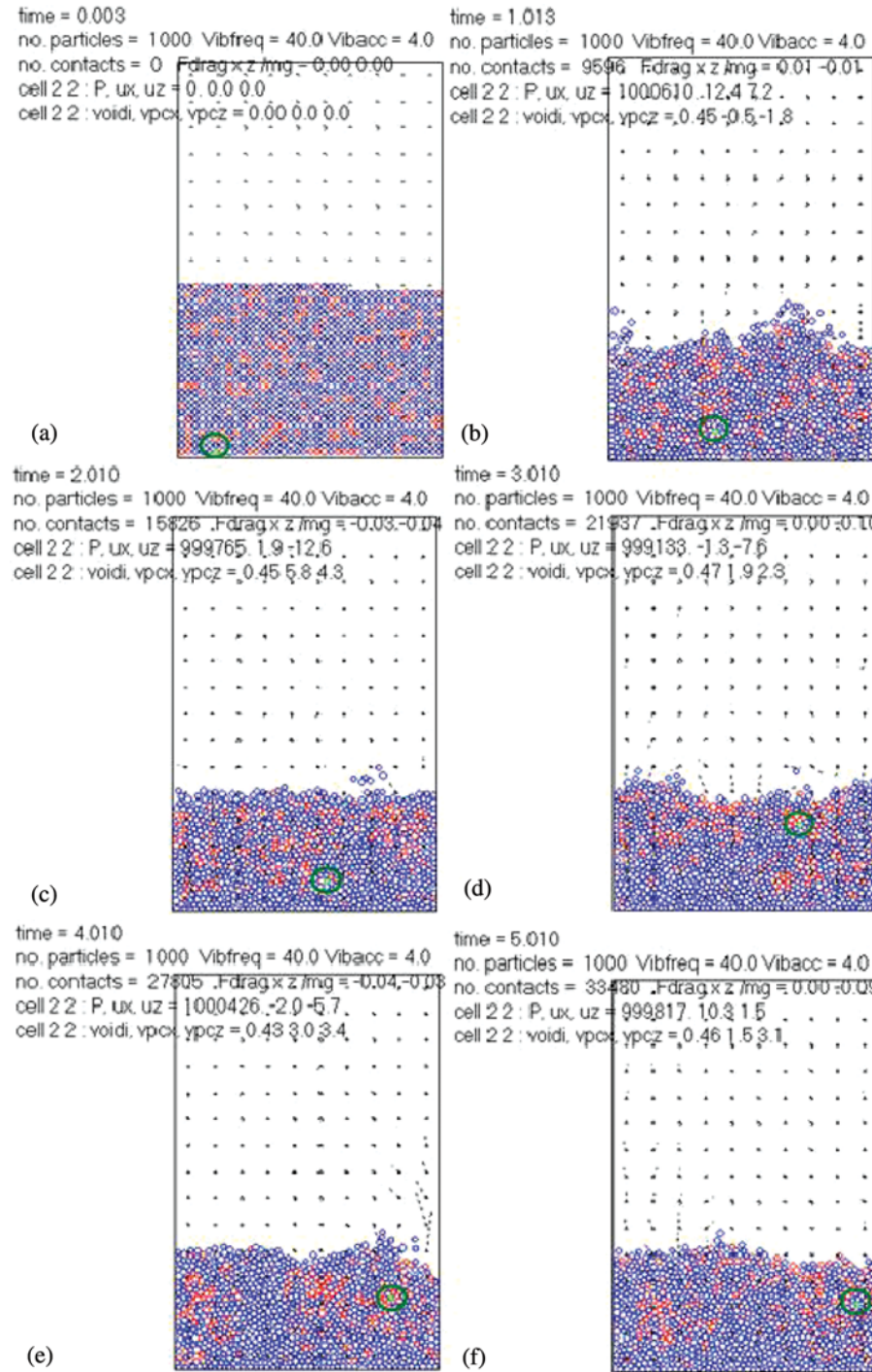


Fig. 8. DEM simulation of time averaged (from a to f, ~ 7.8 sec) segregation progression in an 80:20% number glass and bronze particle Mixture A (Table 3).

5.3 DEM Simulation of Density Segregation in the Glass and Bronzer Particle Mixture A

In an effort to simulate some of the experimentally observed particle segregation conditions such as the ones reported by Burtally et al. (2002; Burtally et al. 2003; Mohabuth and Miles 2005; Mohabuth et al. 2007), the next set of DEM simulation was carried at relatively high vertical vibration frequency and dimensionless acceleration magnitudes and

with particle mixtures that had a high density differential and which reflected the properties of the finely sized glass and bronze particles. The size and composition of the simulated glass and bronze particle mixtures is given in Table 3.

The DEM simulations carried with particle Mixture A (Table 3), which comprised the spherical-shaped glass (70% by number and are shown in blue color) and bronze (20% by number and are shown in red color) particles at the

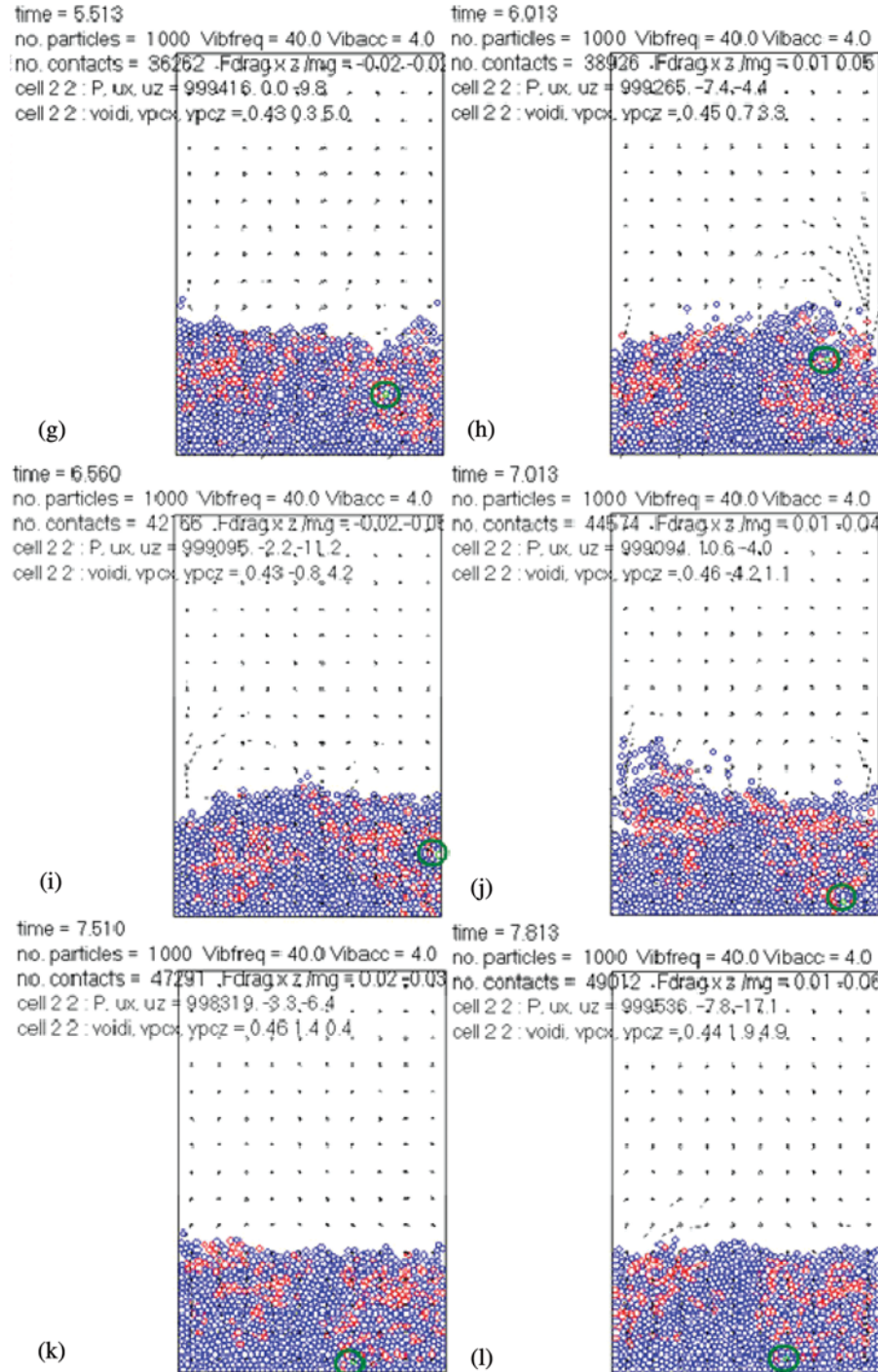


Fig. 8. Continued.

vertical vibration frequency of 20 and 30 Hz and with the dimensionless acceleration magnitudes of 2 and 3 failed to show any significant density segregation potential.

The time averaged progression of vertical vibration induced particle segregation in Mixture A at a vertical vibration frequency of 30 Hz and with a dimensionless acceleration magnitude of 3.5 is snapshot and shown in Figure 7. The green particle in Figure 7 represents a bronze density tracer particle that is introduced into the simulation system

to capture and highlight the distinct movements of the high density particles and is encircled in green for the ease of its detection.

The snapshots in Figure 7a show a randomly well-mixed particle Mixture A (Table 3) that is placed in a rectangular cell and/or container. The vertical vibration is introduced into this container by the up and down movement of the whole container in the z direction as shown in Figure 5. Once all the particles of Mixture A (Table 3) were randomly

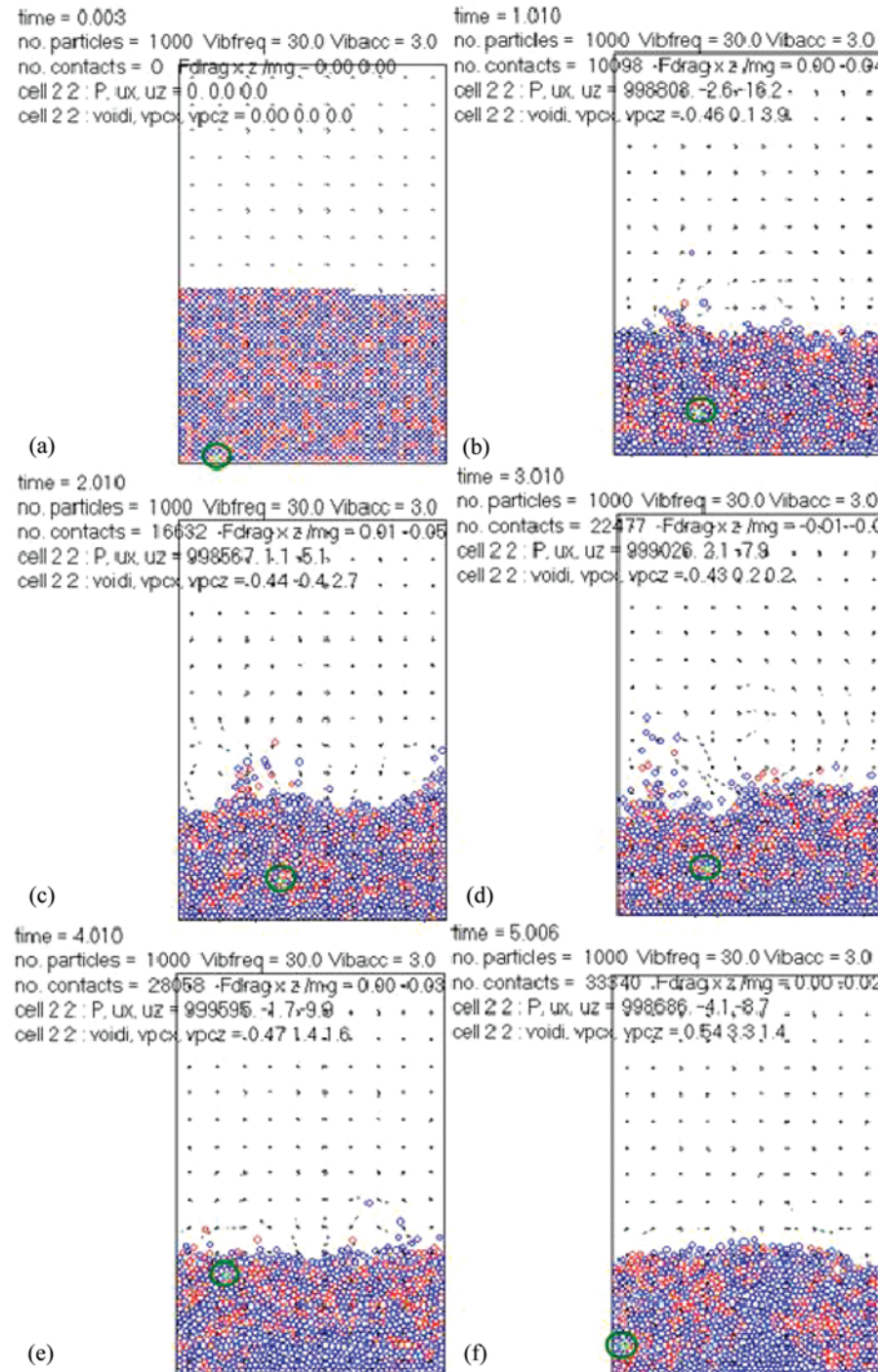


Fig. 9. DEM simulation of time averaged (from a to f, ~5.0 sec) segregation progression in a 70:30% number glass and bronze particle Mixture B (Table 3).

in-placed (in nearly 0.03 sec of the simulation time), the particle mixture was vertically vibrated. This resulted in Figure 7b dynamic particle movements which, in this simulation, lead to the development of identical particle concentration zones. The less stable particle concentration and/or segregation zones (Figures 7c-7f) were mostly observed in the initial simulation stages however, as the simulation time progressed (Figure 7g-7l) the stable local bronze concentrates,

as opposed to the experimental clear cut distinct particle layers reported by Burtally et al. (2002; Burtally et al. 2003), were clearly observed. One of the main reason for the non-observance of clear cut and distinct particle layers in this simulation may be the use of a limited simulation time (10 sec). The simulation time of 10 sec or less was used because of the high levels of CPU demand. This was probably due to the use of a less computational power system for 1000 particles.

Even with 10 sec of simulation run (Figure 8) some interesting particle segregation behaviors were readily observed. The green tracer particle (Figure 7) was initially housed in the bottom layer (Figure 7a) of the particle Mixture A and as the vertical vibration of the container was started (Figures 7b–7d) the green tracer particle was observed to move towards the local high density particle concentrates and gradually started to rise to the vibrated particle bed surface. Once it reached the top particle bed surface, it continued to maintain its motion with the local high density particle concentrates which were mostly developed due to the vertical vibration of the whole system. Overall, the green tracer particle movements showed that it nearly moved to all locations in the vertically vibrated rectangular cell however, the majority of the green tracer particle movements were observed very close to the container boundaries.

Other notable observation was the distinct interstitial gas (air in this case) movement that was introduced from various locations in the vertically vibrated rectangular cell bottom. The air moved through the vibrating particle mixture and showed some distinct convective displacements near to the top particle bed surface as shown in Figure 7.

The time averaged progression of density segregation in the working particle Mixture A (Table 3) which was vertically vibrated at the vertical vibration frequency of 40 Hz and with a dimensionless acceleration magnitude of 4.0 is snapshot and shown in Figure 8.

The DEM simulation results reported in Figure 8 showed similar patterns as seen in Figure 7. The green tracer particle was observed to join the local high density particle concentrates and it moved in a distinct trajectory that was mostly near to the container walls and on top of the particle bed surface. The air currents in this simulation (Figure 8) were observed to be of somewhat stronger magnitude in comparison to what was observed in the simulation reported in Figure 7. Nevertheless, a stable tilt formation and clear-cut particle layer segregation was never observed in this simulation however, stable high and low density particle concentrate formation was readily observed.

5.4 DEM Simulation of Density Segregation in the Glass and Bronzer Particle Mixture B

The time averaged progression of density segregation in the working particle Mixture B (Table 3) which was vertically

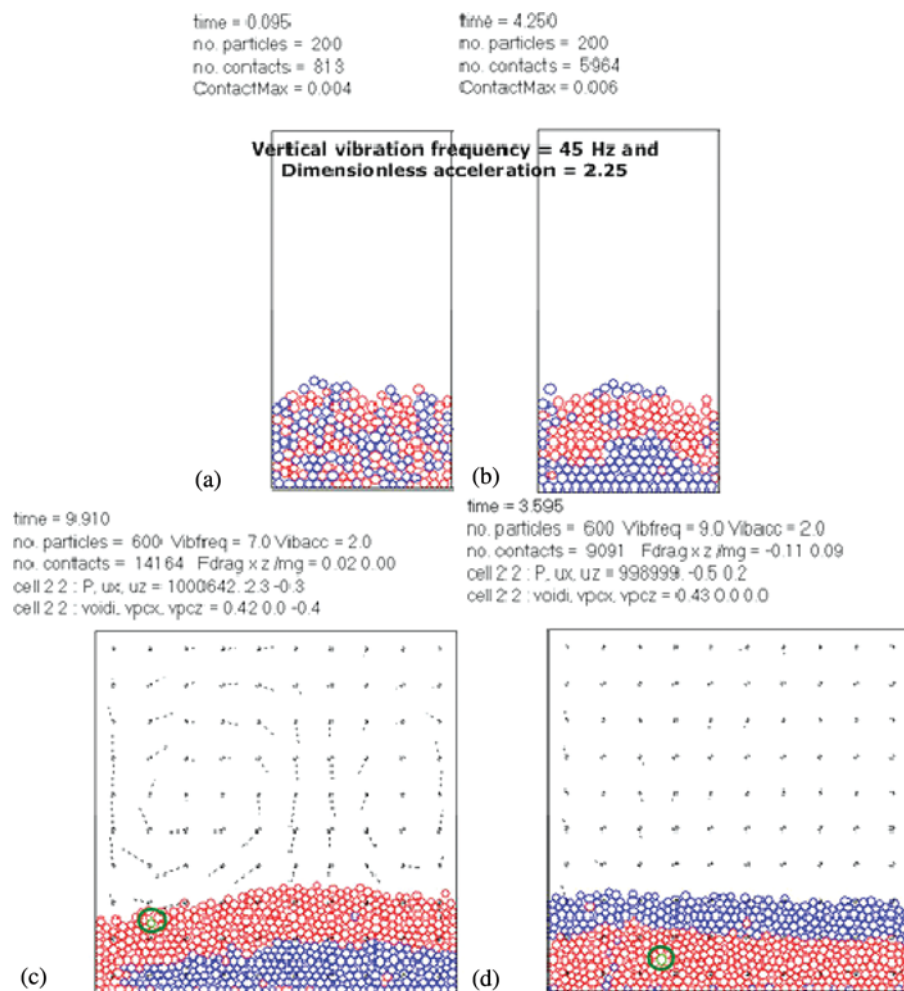


Fig. 10. DEM simulation of particle mixture C (Table 3).

vibrated at the vertical vibration frequency of 30 Hz and with a dimensionless acceleration magnitude of 3.0 is snapshot and shown in Figure 9.

Figure 9 shows that by increasing the number of high density particles to 30% by number, the particle segregation behavior did not improve in nearly 5.0 sec of the simulation run. The segregation trends seen in Figure 9 remained somewhat identical to the patterns reported in Figures 7 and 8.

In Figure 9, the green tracer particle was observed to join the local high density particle concentrates and moved to the top of the particle bed surface however, in this simulation run (Figure 9) the tracer particle did not patrol in the outer particle bed trajectory close to the rectangular cell walls. This tracer particle behavior may be due to the presence of a large number of high density particles that could have affected the vibrated particle bed dynamics.

5.5 DEM Simulation of Density Segregation in the Glass and Bronzer Particle Mixture C

Reducing the number of particles to 200 and 600 in the DEM simulation program resulted in showing some clear-cut high density particles on top and bottom density segregation regimes as shown in Figure 10.

Density segregation in 200 working particles (Figure 10) was observed in nearly 4 sec of the simulation run. This high density particles on top density segregation regime was achieved when the particle Mixture C (Table 3) was vertically vibrated (Figures 10a and 10b) at the vertical vibration frequency of 45 Hz and with a dimensionless acceleration magnitude of 2.25. Under the same conditions of vertical vibration frequency and dimensionless acceleration (45 Hz and 2.25) the increase in the number of particles to 600 did not result in showing any appreciable density segregation. However (Figures 10c and 10d) when the vertical vibration frequency and dimensionless acceleration were dropped to <10 and 2.0 m, respectively (Figure 10c), the formation of high density particle on top and (Figure 10d) bottom particle segregation regimes (Figure 10) were clearly observed.

5.6 DEM Simulation of Density Segregation in the Partitioned Separation Cell

An attempt was made to simulate the prototype scaled partition separation cell reported by Mohabuth et al. (2007).

The working particle mixture used in this work comprised 40% by number of simulated glass (250 μm) particles and 60% by number of bronze (500 μm) particles. The time averaged

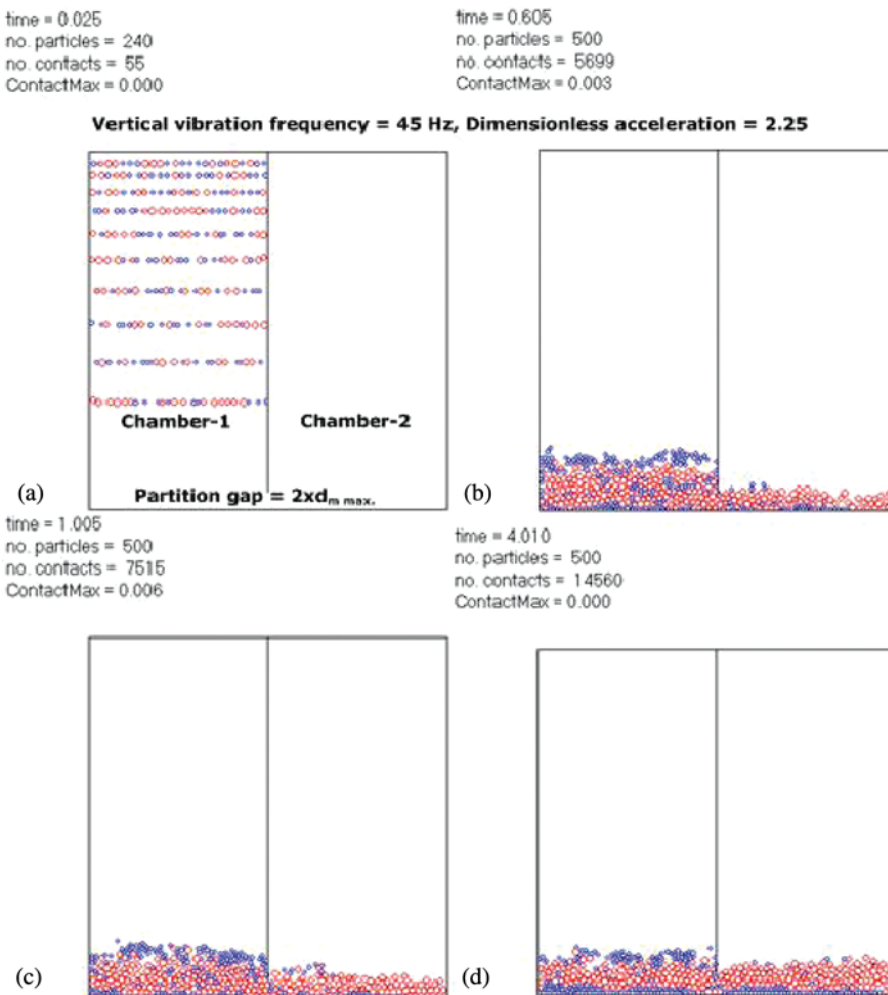


Fig. 11. DEM simulated segregation in a glass (40% by number) and bronze (60% by number) working particle mixture.

progression of density segregation in the working particle mixture that was vertically vibrated at the vertical vibration frequency of 45 Hz and with a dimensionless acceleration magnitude of 2.25 is snapshot and shown in Figure 11.

Figure 11a shows the initial particle charging in chamber-1 of the partitioned container and the particle segregation in chamber-1 and 2 after (Figure 11b) 0.6, (Figure 11c) 1.0, and (Figure 11d) 4.0 sec of the simulation run.

6. Concluding Remarks

In the absence of complete theoretical models, the computer simulations provide a valuable tool to determine the dynamic particle attributes. The DEM model used in this work has shown some elements of convection, tilting, segregation and partitioned particle separation. This simulation has used a maximum of 1000 particles and the particle dynamics is mostly consistent with the experimental work reported in literature (Burtally et al. 2002; Burtally et al. 2003; Mohabuth and Miles 2005; Mohabuth et al. 2007). This work has shown that local high density concentrates can form at high vertical vibration frequency (at and above 30 Hz) and dimensionless acceleration (above 2). The work presented here has provided a useful insight to aid in the further development of a full scale DEM-fluid simulation program.

Acknowledgments

The help and support of Helena Webster is greatly acknowledged.

Funding

M. Habib was supported by the Overseas Research Student and University of Nottingham, UK, Scholarship.

References

- Asmar, B. N., P. A. Langston, A. J. Matchett, and J. K. Walters. 2002. Validation tests on a distinct element model of vibrating cohesive particle systems. *Computers and Chemical Engineering* 26:785–802.
- Biswas, P., P. Sánchez, M. R. Swift, and P. J. King. 2003. Numerical simulations of air-driven granular separation. *Physical Review E* 68:050301/1–050301/4.
- Burtally, N., P. J. King, and M. R. Swift. 2002. Spontaneous air-driven separation in vertically vibrated fine granular mixtures. *Science* 295:1877–1879.
- Burtally, N., P. J. King, M. R. Swift, and M. Leaper. 2003. Dynamical behaviour of fine granular glass/bronze mixtures under vertical vibration. *Granular Matter* 5:57–66.
- Campbell, C. S. 1990. Rapid granular flows. *Annual Review of Fluid Mechanics* 22:57–90.
- Chou, C.-S. 2000. Research on rapid granular flows of highly inelastic particles. *Proceedings of the National Science Council, Republic of China A* 24(5):317–329.
- Fang, X., and J. Tang. 2007. A direct Monte Carlo approach for the analysis of granular damping. *Journal of Computational and Non-linear Dynamics* 2:180–189.
- Fazekas, S. 2007. Distinct element simulations of granular materials. Ph.D. thesis, Budapest University of Technology and Economics, Hungary.
- Fraige, F. Y., and P. A. Langston. 2006. Horizontal pneumatic conveying: A 3d distinct element model. *Granular Matter* 8(2):67–80.
- Gallas, J. A. C., H. J. Herrmann, and S. Sokolowski. 1992. Convection cells in vibrating media. *Physical Review Letter* 69(9):1371–1374.
- Habib, M. 2011. Designing and assessing a novel vertical vibrated particle separator. PhD thesis, University of Nottingham, UK.
- Herrman, H. J., and S. Lüding. 1998. Modelling granular media on the computer. *Continuum Mechanics and Thermodynamics* 10: 189–231.
- Kruggel-Emden, H., E. Simsek, S. Rickelt, S. Wirtz, and V. Scherer. 2007. Review and extension of normal force models for the discrete element method. *Powder Technology* 171:157–173.
- Lee, J. 1994. Heap formation in two-dimensional granular media. *Journal of Physics A* 27:L257–L262.
- Lehon, C. N. B. Cambou, and E. Vincens. 2003. Influence of particle shape and angularity on the behaviour of granular materials: A numerical analysis. *International Journal for Numerical and Analytical Methods in Geomechanics* 27:1207–1226.
- Limtrakul, S., W. Rotjanavijit, and T. Vatanatham. 2007. Lagrangian modelling and simulation of effect of vibration on cohesive particle movement in a fluidised bed. *Chemical Engineering Science* 62:232–245.
- Mohabuth, N., N. J. Miles. 2005. The recovery of recyclable material from waste electrical and electronic equipment (WEEE) by using vertical vibration separation. *Resources, Conservation and Recycling* 45:60–69.
- Mohabuth, N. 2007. The design of a new vertically vibrated particle separator. PhD thesis, University of Nottingham, UK.
- Mohabuth, N., P. Hall, and N. Miles. 2007. Investigating the use of vertical vibration to recover metal from electrical and electronic waste. *Minerals Engineering* 20:926–932.
- Rosato, A. D., D. L. Blackmore, N. Zhang, and Y. Lan. 2002. A perspective on vibration-induced size segregation of granular materials. *Chemical Engineering Science* 57:265–275.
- Taguchi, Y. H. 1992. New origin of convective motion: Elastically induced convection in granular materials. *Physical Review Letters* 69(9):1367–1370.
- Tijssens, E., H. Ramon, and J. D. Baerdemaeker. 2003. Discrete element modelling for process simulation in agriculture. *Journal of Sound and Vibration* 266:493–514.
- Wassgren, C. R. 1997. Vibration of granular materials. PhD thesis, California Institute of Technology. http://thesis.library.caltech.edu/4504/1/Wassgren_cr_1997.pdf (accessed November 11, 2009).
- Yang, S.-C. 1999. Dynamic behaviour of cohesive granular materials in a vibrated bed. Ph.D. thesis, National Central University, Taiwan. http://thesis.lib.ncu.edu.tw/ETD-db/ETD-search/view_etd?URN=85343006 (accessed October 6, 2009).
- Zeilstra, C., M. A. V. D. Hoef, and J. A. M. Kuipers. 2006. Simulation study of air-induced segregation of equal-size bronze and glass particles. *Physical Review E* 74:010302–1–0103024.
- Zhu, H. P., Z. Y. Zhou, R. Y. Yang, and A. B. Yu. 2008. Discrete particle simulation of particulate systems: A review of major applications and findings. *Chemical Engineering Science* 63: 5728–5770.